[Frontiers in Bioscience 19, 1105-1116, June 1, 2014]

Carboxylation-dependent conformational changes of human osteocalcin

Andrea Cristiani[1], Fabio Maset[2], Luca De Toni[3], Diego Guidolin[4], Davide Sabbadin[5], Giacomo Strapazzon[3,6], Stefano Moro[5], Vincenzo De Filippis[2], Carlo Foresta[3]

[1]CRS4, Biomedicine sector, Parco Polaris, 09010 Pula (CA), Italy, [2]Laboratory of Protein Chemistry, Department of Pharmaceutical and Pharmacological Sciences, University of Padova, 35131 Padova, Italy, [3]Department of Molecular Medicine and Centre for Human Reproduction Pathology, University of Padova, 35121 Padova, Italy, [4]Department of Human Anatomy and Physiology, University of Padova, 35121 Padova, Italy, [5]Molecular Modeling Section (MMS), Department of Pharmaceutical and Pharmacological Sciences, University of Padova, 35131 Padova, Italy, [6]EURAC Institute of Mountain Emergency Medicine, 39100 Bozen/Bolzano, Italy

TABLE OF CONTENTS

1. ABSTRACT

Osteocalcin (OCN) is a small noncollagenous protein mainly produced by osteoblasts and is highly represented in bones of most vertebrates. Human OCN contains up to three gamma-carboxyglutamic acid (Gla-OCN) residues at positions 17, 21 and 24 which are thought to increase calcium binding strength, improving mechanical properties of the bone matrix. Recent studies revealed that OCN exerts also important endocrine functions, affecting energy metabolism and male fertility. The latter effect seems to be mediated by the uncarboxylated form of OCN (Glu-OCN). We employed human and mouse OCN as models of fully carboxylated and uncarboxylated OCN forms to investigate, by the use of circular dichroism and molecular dynamics simulations, the respective conformational properties and Ca^{2+} affinity. Ca^{2+} binding was found to trigger a similar conformational transition in both Glu-OCN and Gla-OCN, from a disordered structure to a more compact/stable form. Notably, gamma-carboxylation increases the affinity of OCN for Ca^{2+} by > 30 fold suggesting that, in physiological conditions, Gla-OCN is essentially Ca^{2+}-bound, whereas Glu-OCN circulates mainly in the Ca^{2+}-free form.

2. INTRODUCTION

Osteocalcin (OCN) is a small protein of 46-50 amino acid residues, mainly produced and secreted by osteoblasts. It represents one of the most abundant (10-20%) noncollagenous protein in the bone tissue of most vertebrates examined to date, from bony fish to mammals, and its primary structure is highly conserved among vertebrates (1). In particular, human and porcine OCN contain up to three ?carboxyglutamic acid (Gla) residues at positions 17, 21 and 24 (2). However, the glutamic acid at position 17 (Glu17) is ?-carboxylated only in about 9% of human OCN molecules (3). Carboxylation of Glu-residues is a vitamin K dependent post-translational modification that is thought to increase affinity of OCN for calcium ions (Ca^{2+}) and bone hydroxyapatite, thus contributing to bone formation (4). Circular dichroism and nuclear magnetic resonance analyses indicate that fully γ-carboxylated chicken and bovine osteocalcin (Gla-OCN) in solution are largely unstructured in the absence of calcium (apo-OCN) and that, only after addition of physiological Ca^{2+} concentrations (1.0-1.3 mM), they undergo a transition to a folded state (holo-OCN) displaying highly flexible N- and C-terminal regions characterized by a protein core formed by three α-helical segments stabilized

by a single disulfide bridge, orienting the Gla-residues on the same face of OCN molecule (5-8). Similar conclusions can also be drawn from the crystallographic structures of porcine and fish OCN (9-10).

Notably, Ca^{2+}-free OCN (apo-OCN) can be detected in circulating plasma and its levels are generally associated with higher osteoblast activity and increased bone formation (11). Recent studies, performed on animal models, revealed that OCN not only exerts structural function in the bone but has also important endocrine functions, affecting energy metabolism, bone mass growth and male fertility (12-16). In fact *OCN*$^{-/-}$ null mice, together with bone disorders, display accumulation of visceral fat associated with insulin resistance, glucose intolerance, and poor fertility. The latter pathological state is associated with decreased serum testosterone (16). Furthermore, deletion of *Esp*$^{-/-}$, a gene encoding for the protein tyrosine phospatase involved in ?-carboxylation of OCN, resulted in a gain of OCN bioactivity on insulin, adiponectin and testosterone regulation, leading to severe hypoglycemia, protection against diet-induced obesity and diabetes together with a higher expression of enzymes involved in testosterone biosynthesis (16). Similar effects were obtained with the fully decarboxylated form of OCN (Glu-OCN) by its interaction with GPRC6A, a member of the G Protein Coupled Receptor superfamily (16-18). Thus the γ-carboxylation status of Glu-residues within OCN structure appears to exert dramatic consequences on OCN function, by regulating the equilibrium between the concentration of Gla-OCN, playing a major structural role in bone formation, and Glu-OCN, exerting a key hormonal role in male fertility and energy metabolism (19).

In the light of these considerations, circular dichroism (CD) and molecular dynamics (MD) simulations were used to study the conformational properties and sensitivity to Ca^{2+} of apo- (i.e., Ca^{2+}-free) and holo-OCN (Ca^{2+}-bound) in the fully γ-carboxylated (Gla-OCN: Gla-residues at positions 17, 21 and 24) and uncarboxylated (Glu-OCN: Glu-residues at positions 17, 21 and 24) state. The results of the conformational analysis reported herein set a clear correlation between the extent of γ-carboxylation and the molar fraction of apo-OCN existing under physiological conditions in human OCN.

3. MATERIALS AND METHODS

3.1. Analytical techniques

Human Gla-OCN and murine Glu-OCN were purcahesed by Bachem (Bubendorf, Switzerland) and their purity and chemical identity was checked by RP-HPLC and mass spectrometry. An aliquot (20 μg) of human Gla-OCN was loaded onto a Vydac C18 column (4.6×250 mm, 5μM) (Hesperia, CA, USA) eluted with an acetonitrile-0.078% TFA gradient from 20 to 60% in 30 min at the flow rate of 0.8 ml/min. Mass spectrometry analysis was carried out on a Mariner (PerSeptive Biosystems, Stafford, TX, USA) ESI-TOF spectrometer, yielding mass values in agreement with theoretical mass within 50 ppm accuracy.

3.2. Spectroscopic techniques

Binding of calcium to human or murine OCN was studied by far-UV circular dichroism (CD) spectroscopy. Aliquots (2-50 μl) of a $CaCl_2$ stock solution (150 mM) were added under gentle magnetic stirring to a solution of OCN (1.5 ml; 20 μg/ml) in a 1-cm pathlength cuvette. Ellipticity data are expressed as mean residue ellipticity , $[\theta] = (\theta \cdot MRW)/(10 \cdot l \cdot c)$, where θ is the measured ellipticy in degrees, MRW is the mean residue weight, l is the cuvette pathlength (1 cm) and c is the protein concentration in g/ml. All measurements were carried out in 20 mM Tris-HCl, pH 7.4, at 25±0.2 °C on a J-810 spectropolarimeter (Jasco, Tokyo, Japan) equipped with a thermostated cell holder and Peltier PTC-423S temperature control system. Each spectrum was the average of four accumulations, after base line subtraction. Data points were fitted using the equation:

$$(\text{eq. 1})\ \theta = \theta_0 + [\theta_{max} \cdot ([Ca^{2+}]/K_d))/(1+[Ca^{2+}]/K_d)$$

where θ_0 and θ_{max} are the ellipticity values of OCN in the absence and at saturating calcium concentration, respectively, and K_d is the dissociation constant of the complex Ca^{2+}-OCN.

3.3. Thermal stability measurements

The thermal unfolding of Glu-OCN and Gla-OCN was monitored by recording the decrease in the CD signal at 222 nm as a function of the sample temperature, applying a heating rate of 60 °C/h, as detailed elsewhere (20). Thermal denaturation measurements were carried out at 20 μM Glu-OCN and Gla-OCN. For the holo-forms, a saturating concentration of 30 mM $CaCl_2$ was used with Glu-OCN and 5 mM with Gla-OCN. Both CD signal and temperature data were recorded simultaneously using the "variable temperature" software (Jasco, Easton, MD, USA). The reversibility of the thermal unfolding process was determined by measuring the recovery of the CD signal upon cooling to the starting temperature (i.e. 5 °C). Thermal denaturation curves were analyzed within the framework of a two-state model for the N ? U transition. At a given temperature, T, only native, f_N, and unfolded, f_U, fractions of the protein are present at significant concentration, such that $f_N + f_U = 1$. The observed CD signal, y, is given by the equation $y = y_N \cdot f_N + y_U \cdot f_U$, where y_N and y_U are the CD signal values characteristic of the native and unfolded state at that T, respectively. For each T in the transition region, it is possible to calculate the the equilibrium constant, $K_U = (y_N - y)\ (y - y_U)$ and the free energy change for the unfolding reaction $\Delta G_U = -RT \cdot \ln K_U$, where R is the gas constant (8.134 $J \cdot mol^{-1} \cdot K^{-1}$). The melting temperature, T_m, defined as the temperature at which the concentrations of the native and unfolded species are identical (i.e., $\Delta G_U = 0$), was derived from the linear regression equation obtained by plottin ΔG_U vs T in the transition region. The entropy, ΔS_m, and the enthalpy, ΔH_m, changes of unfolding at T_m were calculated according to the equations $\Delta S_m = -d\Delta G_U/dT$ and $\Delta H_m = T_m \cdot \Delta S_m$, respectively.

3.4. Homology modeling

The three-dimensional model of the human osteocalcin was carried out using a conventional homology modeling approach implemented in the MOE suite and

using as a structural template porcine OCN, (PDB code: 1Q8H) (9, 21). Hydrogen atoms and electric charges were added using the "Protonate-3D" tool implemented in MOE. To minimize contacts among hydrogens, the structures were subjected to Amber94 force field minimization until the *rmds* of conjugate gradient was <0.1 kcal/mol/Å, keeping heavy atoms fixed at their crystallographic positions (22). The model quality was evaluated using the MOE stereochemical quality evaluation tool. The atomic coordinates of MD models will be made available upon request to the corresponding author.

3.5. Molecular dynamics

tLeap and Amber FF99SB were employed for the parametrization of the protein models of Gla-OCN and Glu-OCN (23, 24). Gla-residues were parametrized "from scratch" using molecular information from the available crystal structures, while Ca^{2+}-ions were parametrized as detailed elsewhere (25). The protein models were equilibrated in TIP3P water boxes and finally added counterions (i.e. Na^{+}) to assure the neutrality of the molecular systems.

Analysis of trajectories was performed with VMD 1.8.7, RMSD Trajectory Tools 2.01, RAINBOW-RMSD and NRGPLOT (26-28). Steered molecular dynamics (SMD) simulations were run us to obtain an estimate of the binding strength of Ca^{2+}-OCN complexes (29). In our simulations a constant acceleration (35.000 pm/ps^2) was applied to Ca^{2+}.

4. RESULTS

4.1. Effect of g-carboxylation on the conformation and affinity of OCN for calcium

The conformational properties of Glu-OCN and Gla-OCN were investigated by CD spectroscopy in the far-UV region (Figure 1 A), which is a sensitive probe of protein secondary structure (30). In the absence of calcium, both spectra shared a similar shape, with a minimum at 204-208 nm and a shallow band at 220 nm, indicating that both polypeptide chains were rather flexible and disordered, but that they also containd some nascent helical structure. Human Gla-OCN, however, displayed a more intense signal at 220 nm, that could reflect a higher α-helix content of Gla-OCN, compared to Glu-OCN. Alternatively, these differences could be merely spectroscopic and thus reflect the different contribution of the aromatic amino acids in the two proteins (30). With respect to this point, human Gla-OCN contains 5 Tyr, 2 Phe and 1 Trp, whereas mouse Glu-OCN only contains 4 Tyr (Figure 3 C).

The effect of γ-carboxylation on the affinity of OCN for calcium was investigated by recording the CD spectra at increasing [Ca^{2+}] (Figure 1, C and D) and plotting the CD signal at 222 nm as a function of [Ca^{2+}] (Figure 1 B). As shown in Figure 1 A, at saturating [Ca^{2+}], both the shape and intensity of the spectra were changed and more closely resembled those of proteins with high helical secondary structure, with two minima at 208 and 222 nm (30). These data provided clear-cut evidence that addition of Ca^{2+} caused both Glu-OCN and Gla-OCN to fold into a more ordered helical conformation, in agreement with previous CD measurements obtained with chicken and bovine OCN (5-7). Interpolation of the data points in Figure 1 B with equation 1 yielded a dissociation constant, K_d, for the Ca^{2+}-OCN complex of 0.11 ± 0.01 mM for human Gla-OCN and 3.64 ± 0.23 mM for mouse Glu-OCN. These data show that γ-carboxylation of Glu-residues markedly increases the affinity of OCN for calcium by > 30 fold and suggest that at physiological concentrations of Ca^{2+} in the serum (1.03 – 1.30 mM) (31) > 90% of Gla-OCN is saturated with Ca^{2+}, whereas at the same concentration only ~ 30% of Glu-OCN is in the Ca^{2+}-bound form. Accordingly, comparing the CD spectra of apo- and holo-OCN in Figure 1 A, we conclude that Glu-OCN and Gla-OCN may have remarkably different conformations in the plasma, with Gla-OCN being more helical and compact whereas Glu-OCN more flexible and disordered.

4.2. Effect of g-carboxylation on the stability of OCN in the apo- and holo-form

The stability of Glu-OCN and Gla-OCN was studied in the presence and absence of saturating concentrations of Ca^{2+}, i.e. 30 mM for Glu-OCN and 5 mM for Gla-OCN, by recording the decrease in the ellipticity at 222 nm at increasing temperatures (Figure 2). The reversibility of thermal unfolding was > 90%. From the denaturation curves in Figure 2A the value of the melting temperature, T_m, could be estimated, according to a two-state unfolding mechanism (Figure 2 B). Our data showed that, in the absence of Ca^{2+}, the unfolding of Glu-OCN is barely cooperative with a T_m = 34±0.5 °C, even lower than the physiologically relevant temperature (37°C). In the presence of 30 mM Ca^{2+}, the denaturation curve of Glu-OCN had a sigmoidal shape, indicative of a cooperative unfolding (32) and T_m increased by approximately 12°C (T_m = 45.4±0.5°C). Interestingly, in the absence of Ca^{2+}, the T_m of Gla-OCN was > 14°C higher (T_m = 48±0.3°C) than that of Glu-OCN. After adding saturating Ca^{2+} concentration, i.e. 5 mM, the T_m of Gla-OCN increased by 12°C (T_m = 60±0.2°C), similarly to what observed with Glu-OCN. Our data unequivocally indicate that Gla-OCN is intrinsically more stable than Glu-OCN, regardless of calcium, and that saturating concentrations of Ca^{2+} enhance the T_m of OCN to a similar extent, regardless of γ-carboxylation. The stabilizing effect of Ca^{2+} binding is coherent with the notion that the metal ion selectively binds to the native state rather than to the unfolded state (33-35). The higher stability of Gla-OCN can be explained considering that, whereas five Pro-residues are conserved among human Gla-OCN and mouse Glu-OCN, the γ-carboxylated OCN has two extra prolines, Pro9 and Pro48, compared to the uncarboxylated form (Figure 3 C). The presence of a highly conformationally constrained amino acid such as Pro at the fraying N- and C-terminal regions of OCN likely stabilizes the protein by preferentially rigidifying the unfolded state (36, 37).

4.3. Homology modeling of human OCN

Considering the high sequence identity (88%) (Figure 3 A) existing between porcine and human OCNs and the conservation of the crucial ExxxExCExxxxC motif

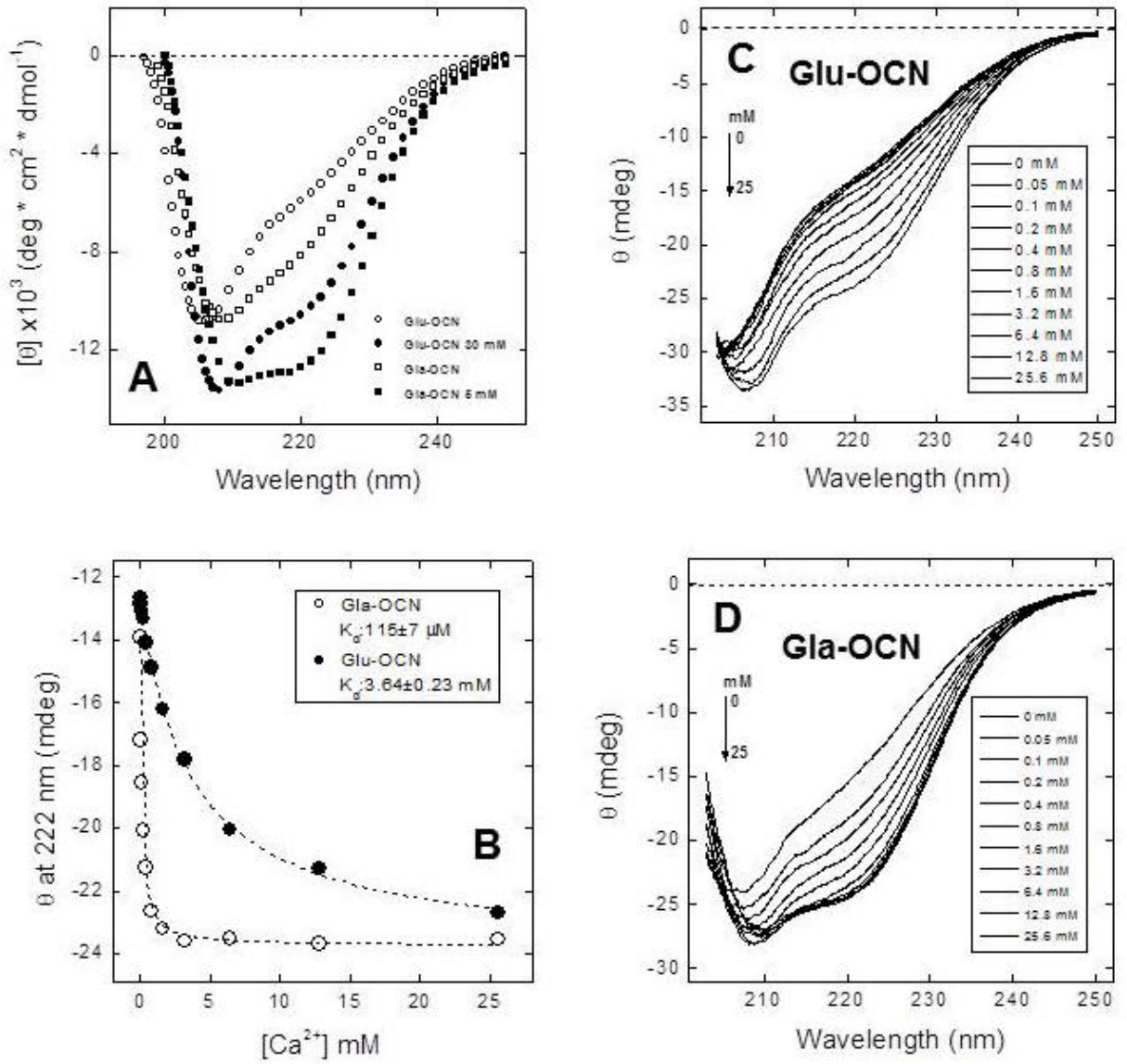

Figure 1. (A) Far-UV circular dichroism spectra (CD) spectra of Glu-OCN and Gla-OCN in the absence and presence of saturating Ca^{2+} concentration, as indicated. CD spectra of Glu-OCN (B) and Gla-OCN (C) in the presence of increasing Ca^{2+} concentrations. (D) Plot of the ellipticity value at 222 nm as a function of [Ca^{2+}] for Glu-OCN (?) and Gla-OCN (?). The data points were fitted with equation 1 and a K_d value could be calculated as 115 µM for the binding of Ca^{2+} to Gla-OCN and 3.64 mM for the binding of Ca^{2+} to Glu-OCN. All measurements were carried out in 20 mM Tris-HCl, pH 7.4, at 25±0.2 °C.

in the two proteins, a homology model of human OCN was built starting from the crystallographic structure of porcine osteocalcin (PDB code: 1Q8H) (9). Because of the high conformational flexibility of the N-terminal region in the template structure, only the amino acid residues from Pro13 to Val49 could be modelled.

The resulting human OCN model (Figure 3 B) displayed three helices H1(Asp14-Leu25), H2(Asp28-Ile36), and H3(Gln39-Tyr46), stabilized by numerous hydrogen bonds (HB) involving Asp14, Gla17 and Arg20 in H1 helix, Glu31 and His35 in the H2 helix, and Glu40 and Arg43 in H3 helix. The orientation of H1 and H2 was locked by a disulfide bridge between Cys23 and Cys29 in the protein core.

A distinctive structural feature of human OCN entailed the asymmetric distribution of positive and negative amino acids within the model structure. In particular, a wide negatively charged surface was generated by clustering of acidic amino acids in H1 (Gla17, Gla21 and Gla24) and H2 helix (Asp28, Asp30, Glu31 and Asp34), whereas a few positively charged amino acids (Arg19, Arg43 and Arg44) was located on the opposite face

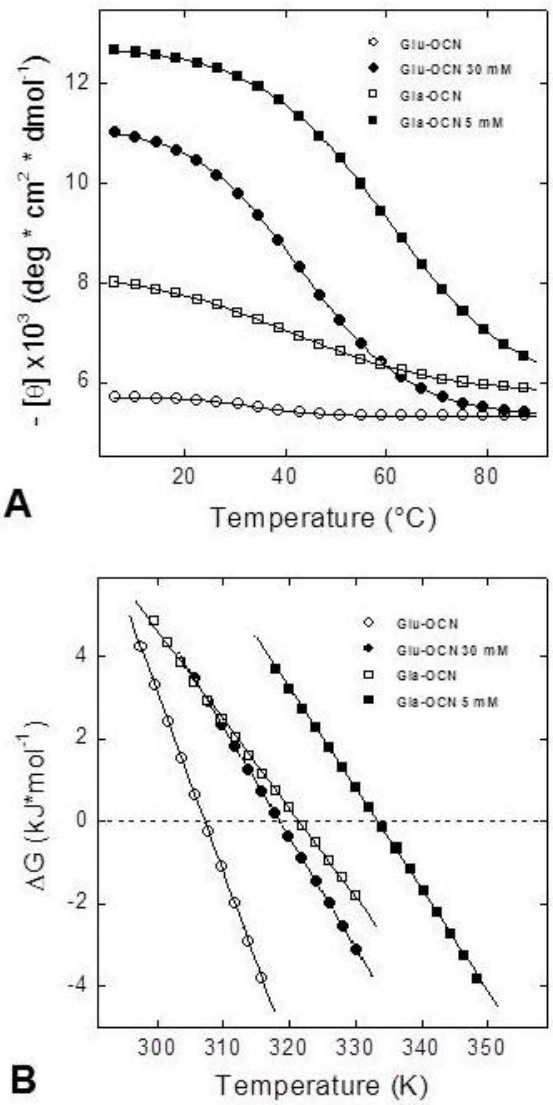

Figure 2. (A) Thermal denaturation of Glu-OCN and Gla-OCN in the presence or absence of saturating [Ca^{2+}], as indicated. The unfolding process was followed by recording the CD signal at 222 nm as a function of the sample temperature at identical OCN concentrations in 20 mM Hepes buffer, pH 7.4 phosphate buffer (Methods). (B) Temperature dependence of the free energy change, ΔG_U, for the denaturation of Glu-OCN and Gla-OCN in the apo- and holo-form, as indicated. The thermodynamic data were calulated within the approximation of a two-state model (Methods).

of the protein. As shown in Figure 3 B, clustering of negative amino acids was instrumental for the binding of three Ca^{+2} ions.

4.4. Molecular dynamics simulations and calcium binding to Glu-OCN and Gla-OCN

Classical molecular dynamics (MD) simulations were performed on two different carboxylation state models of human OCN: Gla-OCN, containing three Gla-residues at position 17, 21 and 24 and Glu-OCN in which all Gla-residues were replaced by Glu.

4.4.1. Gla-OCN

At the beginning of the simulation, the C-terminal end of the protein pointed into the bulk solvent, while after 1 ns it interacted with Tyr42. After 10 ns it made a stable interaction with Arg19 (Figure 4, A and B). The latter interaction was broken at 34 ns and after 50 ns it was reformed and then remained stable until the end of the simulation at 100 ns. This final stabilization was due to the participation of Gln39 in the chemical environment, after 67 ns of MD. The three Ca^{2+} ions were coordinated by Gla21, Gla24, Asp30, and Glu31 forming a "carboxy-cage" bridging H1 to H2 helix via Ca^{2+} bonds. Notably, Gla17 did not seem to participate in Ca^{+2} binding, consitently with the low frequency of γ-carboxylation (9%) occurring at this position in human OCN (3).

4.4.2. Glu-OCN

When the same simulation protocol was applied to the uncarboxylated Glu-OCN model, (Figure 4, C and D) disruption of the polar interaction between the C-terminal carboxylate group and Arg43 side chain (after 21 ns) and a subsequent (after 24 ns) hydrogen bond formation, between Gly47 backbone and Tyr42 side chain, was observed. This last interaction caused the re-orientation of the C-terminal end toward Arg19 side chain but, at variance with what observed with Gla-OCN, no stable interaction was formed at this stage. After 34 ns of simulation, the Gly47-Tyr42 hydrogen bond was broken and after 48 ns the C-terminal oriented toward Arg19. In this condition, the C-terminal carboxylate formed a stable polar interaction with Arg19, which was stabilized by Tyr42. The latter conformation was detectable until the end of MD simulation. Conversely from what we observed with Gla-OCN, Gln39 was not involed in the stabilization of the C-terminal conformation.

In the Glu-OCN model, the Ca^{2+} ions were coordinated by Glu21, Glu24, Asp30, Glu31, and Asp34. The initial interaction between the side chains of Glu31 and His35 was broken and replaced by Glu31-Ca^{2+}-Asp34 coordination. Generally, Ca^{2+} ions moved less when compared to the Gla-OCN model. Moreover, the "carboxy-cage" of Glu-OCN model oriented the 3 Ca^{2+} ions in a different conformation compared to the Gla-OCN model, the major difference being in the coordination of Ca^{2+} by Glu24 and Asp30 in Glu-OCN (Figure 4, C and D). After 25 ns of MD simulation, the different calcium-binding network enabled Phe38 in Glu-OCN model to flip around the Cα-Cβ bond, thus filling a hydrophobic pocket formed by Ala33 side chain, the Arg20 methylene-groups and the disulfide bridge Cys23-Cys29.

The effect of the Ca^{2+} ions in the Gla-OCN and in the Glu-OCN models was monitored by analysing the protein root mean square deviation (RMSD) over 100 ns of large-scale NVT molecular dynamics simulation (Figures 5 and 6). Both the RMSD plot and the heatmaps of Gla-OCN and Glu-OCN in the presence of Ca^{2+} ions indicated a markedly lower conformational flexibility compared to the simulations run in the absence of Ca^{2+}. This effect was

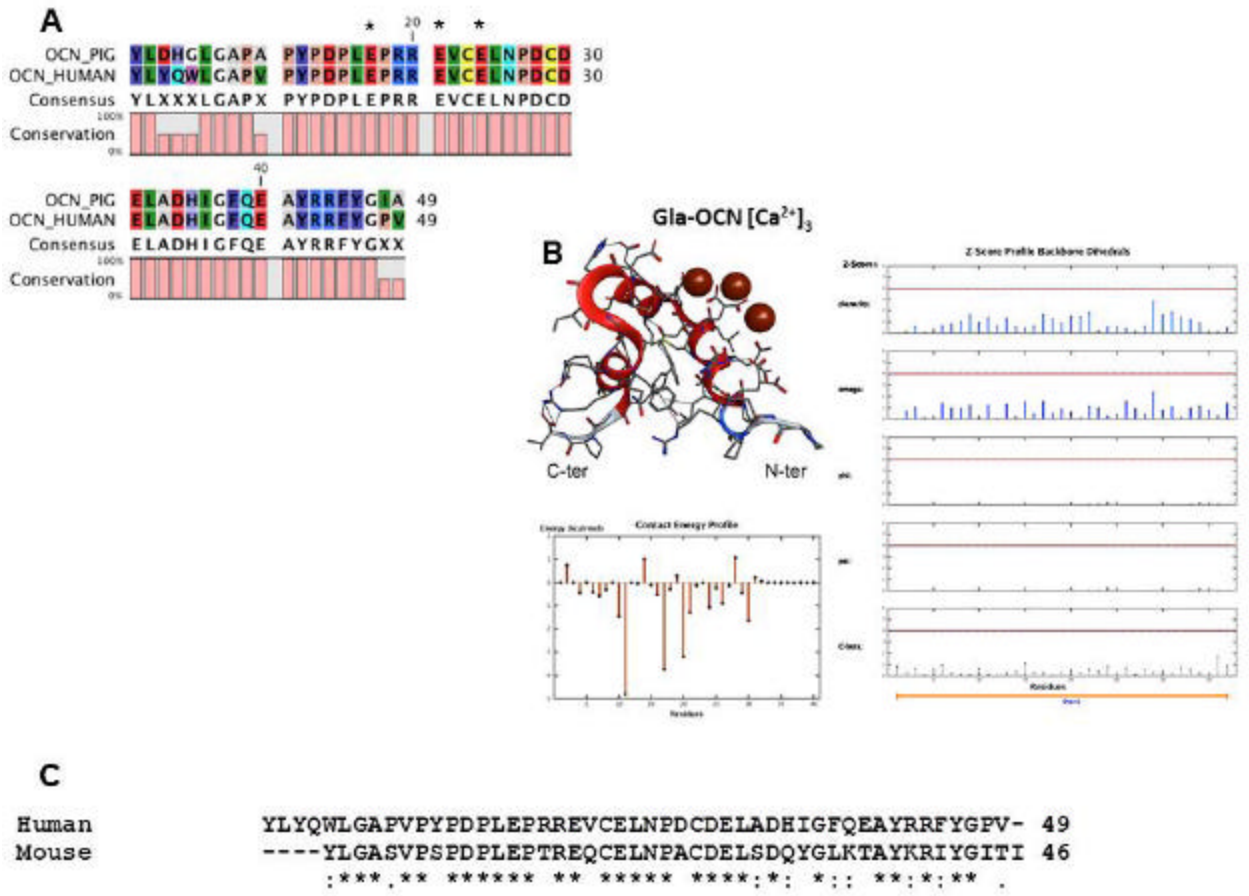

Figure 3. Sequence alignment of human OCN with porcine (A) and murine (B) OCN. Threedimensional model of Gla-OCN-holo, as obtained by homology modelling.

particularly evident with Glu-OCN and a plausible explanation could be searched in the involvement of the counter ions added to the molecular system during the molecular dynamics parameterization. Gla-OCN had three carboxylate-groups more than Glu-OCN, whose effect was balanced by three Na+ ions, which were not present in the Glu-OCN molecular system. In conclusion, our data suggest that in the absence of Ca^{2+}, OCN can explores a larger conformational space compared to the Ca^{2+}-bound form, both with the γ-carboxylated and uncarboxylated forms.

4.5. Steered molecular dynamics

Starting from the average OCN structures obtained during MD trajectories, further investigations were carried out through steered molecular dynamics (SMD) simulations applied on the complexes between Ca^{2+} ion and the two carboxy-states of OCN, as shown in Figure 7 A and B. SMD simulations allowed us to give a rough and fast evaluation of the strength of the binding between Ca^{2+} and OCN forms. Briefly, during SMD simulations an external force was applied to a ligand, in a protein complex, to facilitate its unbinding from a protein. Thereafter, analysis of interactions of the dissociating ligand with its binding region, as well as recording of applied forces as a function of time and ligand position, has proven to provide key insights on the structure-function relationships of ligand-receptor complexes and binding pathways (29). Interestingly, based on the degree of carboxylation of the protein, different "distance profiles" were obtained (Figure 7 C). There was a clear qualitative correlation between the degree of carboxylation of the protein and the strength of Ca^{2+} binding. In fact, using the same external acceleration on the Ca^{2+} ions (35.000 pm/ps2), in the uncarboxylated Glu-OCN the unbinding process appeared after 7 ps, whereas in the the ?-carboxylated Gla-OCN the unbinding process took place only after 42 ps of SMD simulation. The comparison of the two curves in Figure 7 C indicates that a stronger force is required for Gla-OCN model to reach the same distance from the protein, thus suggesting that the strength of the interaction between the Ca^{2+} and OCN depends on the degree of carboxylation of the protein. These results favourably compare with experimental data showing that the affinity of Ca^{2+} for OCN is >30 fold higher with the fully carboxylated Ga-OCN (K_d = 0.11 ± 0.01 mM) than with the uncarboxylated Glu-OCN (K_d = 3.64 ± 0.23 mM) (Figure 1 B)

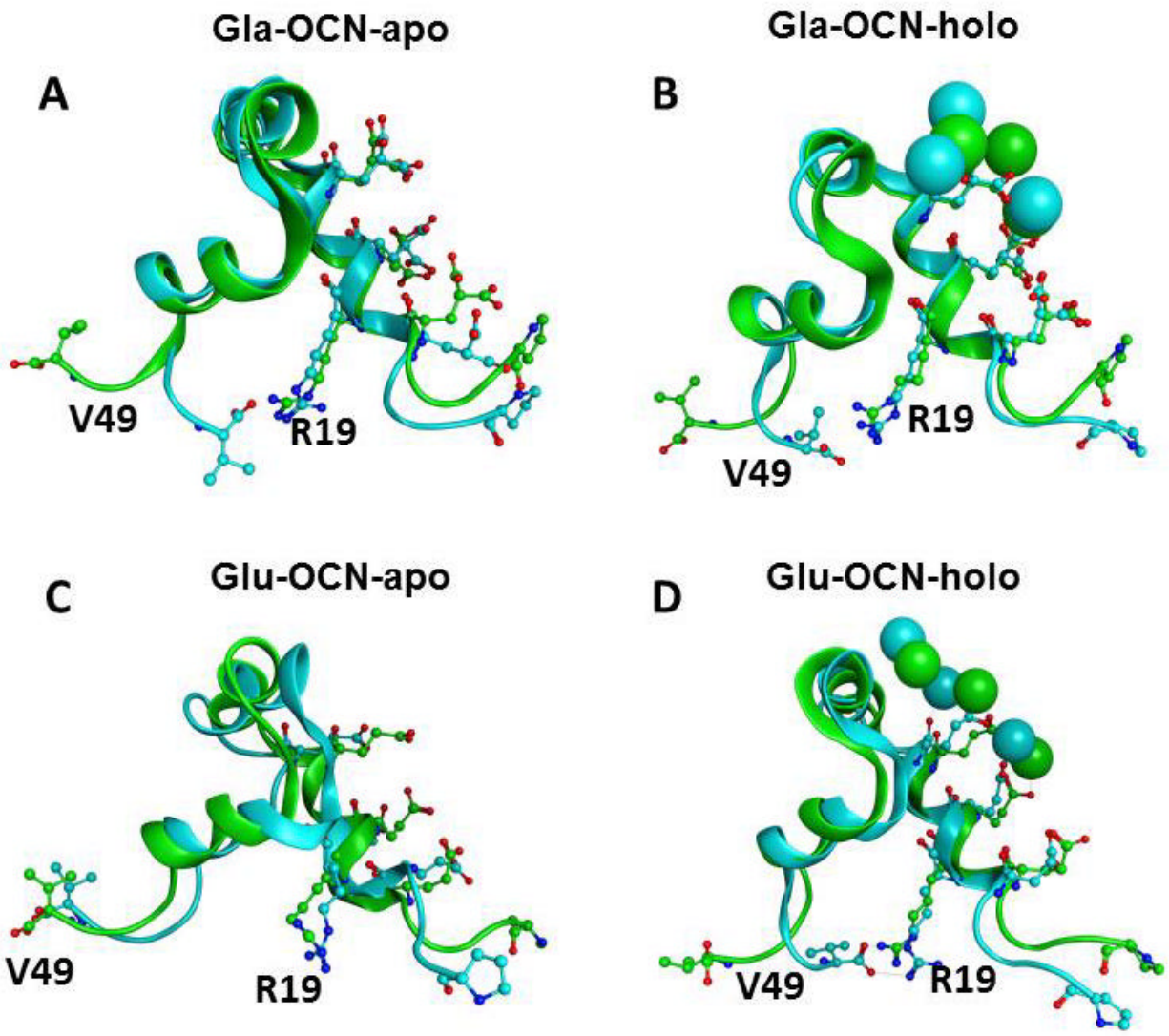

Figure 4. (A-B) Superimposition of Gla-OCN in the apo (A) and holo (B) at the beginning (green) and after 100 ns molecular dynamics simulation (cyan). (C-D) Superimposition of Glu-OCN in the apo (C) and holo (D) at the beginning (green) and after 100 ns molecular dynamics simulation (cyan).

5. DISCUSSION

Osteocalcin influences bone mineralization partly through its ability to bind with high affinity to the mineral component of bone HA (9). Recent studies on porcine OCN revealed an excellent surface complementarity between the Ca^{2+} coordinating surface of OCN and the prism face of HA, suggesting that OCN may also show selective binding characteristics to HA (9). Our results extend this behaviour about Ca^{2+} affinity to human OCN and, interestingly, the Ca^{2+}-binding-related increase of a-helical secondary structure observed in our study, reflects the observation of Nishimoto *et al.* in fish OCN, similarly describing the relative increase in a-helical content of teleost osteocalcin upon Ca^{2+} binding (38). Calcium ions, in fact, appear to have a role in stabilizing the protein conformation through its electrostatic interaction with negative charges within a "carboxy-cage", involving amino-acids at positions 21, 24, 30 and 31 for both forms of OCN. Interestingly, molecular dynamics analysis suggests low or negligible participation of Gla17-residue to Ca^{+2} binding, consistently with the low frequency of γ-carboxylation (9%) occurring at this position in human OCN (3). In agreement with computational analysis, experimental data of the current study describe a calcium-dependent increase of CD signal at 208 and 222 nm, likely attributable to the described up-representation of alpha-helical secondary structure (5-7).

Moreover, we describe for the first time the different biochemical characteristics of uncarboxylated OCN, inferring about its possible implication in OCN-endocrinological activity. Lee *et al.* showed how mice osteoblasts cultured with warfarin, an inhibitor of ?

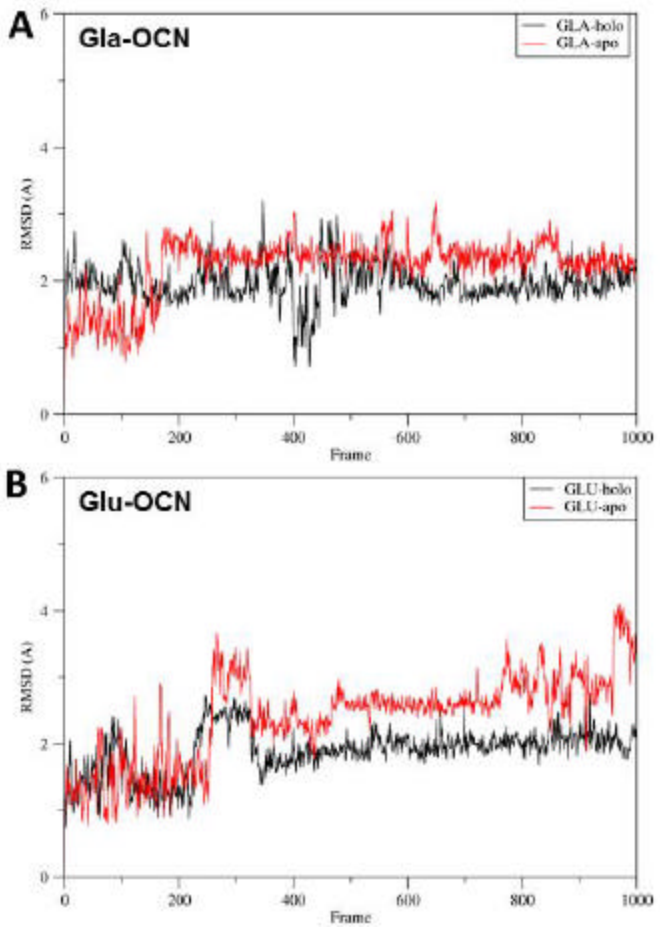

Figure 5. (A) Superposition of the RMSD trace over time of the Cα-atoms in Gla-OCN in the apo (red) and holo (black) form during 100 ns MD simulations. (B) Superposition of the RMSD trace over time of the Cα-atoms in Glu-OCN in the apo (red) and holo (black) form during 100 ns MD simulations.

carboxylation, led to a significant decrease in the percentage of osteocalcin bound to HA (12). On the other side, conditioned medium from warfarin-treated osteoblasts induced higher expression of adiponectin in adipocytes, compared to vehicle-treated osteoblasts. (12). Only uncarboxylated OCN, in cell-based *in vitro* assays, could induce expression of *Adiponectin* in adipocytes, and of *Insulin* and *CyclinD1*, in islets β-cells (12). In the former model, no effects were demonstrated by stimulation with osteocalcin featured by fully carboxylated Gla-residues. Data from Ferron *et al.* confirmed such an evidence. In fact, when rat insulinoma INS-1 cells were treated with carboxylated OCN (i.e. at pH 7.5) or undercarboxylated OCN (i.e. at pH 4.5), only the latter form could increase insulin secretion to the same extent of recombinant uncarboxylated OCN (i.e. of recombinant production), used as a positive control (13). Similar results were shown by Oury *et al.* through testosterone production by Leydig cells, partially explaining both results observed in *in vivo* models and studies performed on humans affected by dismetabolic conditions, such as diabetes, obesity and hypogonadism, the latter showing a reduction of serum ucOCN/total OCN ratio (15, 16). The human Glu-OCN obtained through homology modelling based on 1Q8H porcine template displayed features similar to those previously described for the Gla-OCN model (9). Protein structures of both forms displayed high conformational changes in N-terminal and especially in the C-terminal, greatly depending from interactions among Gla-residues and with Ca^{2+}. In fact, data from RMSD plot and heatmap analysis revealed that both Gla-OCN and Glu-OCN experience lower conformational spaces in presence of Ca^{2+}, compared to the simulations of the same proteins in absence of Ca^{2+} ions. Interestingly, the experimental session showed that the degree of ?-carboxylation of glutamic acid residues significantly modifies calcium affinity of OCN, in agreement with the molecular dynamics data. In fact, data from thermal variations in the ellipticity evidenced how calcium-binding confers an overall stability to the whole molecule of OCN, in particular for Gla-OCN. Gla-OCN showed to have higher affinity for calcium compared to the Glu-OCN, with a difference, in terms of K_d, of more than 30 fold higher. Given an average extracellular calcium concentration of 1.03 – 1.30 mM , Gla-OCN would result almost entirely

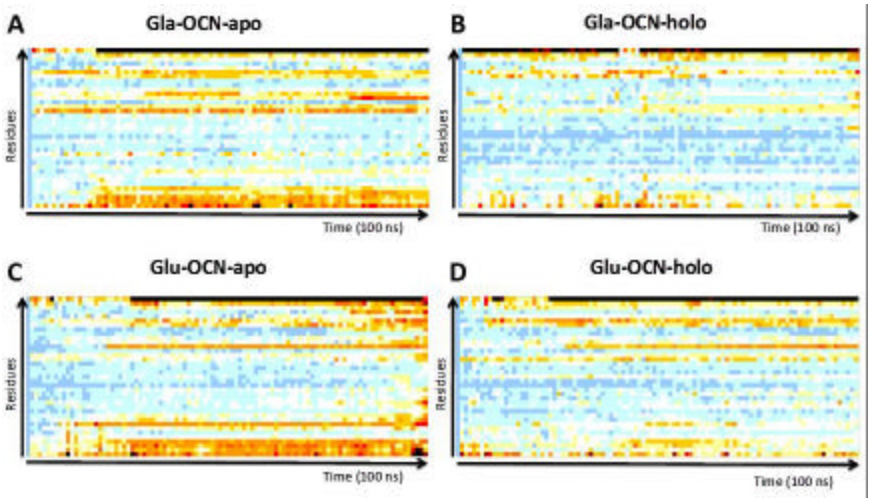

Figure 6. Flexibility heatmaps of Gla-OCN-apo (A), Gla-OCN-holo (B), Glu-OCN-apo (C), and Glu-OCN-holo (D).

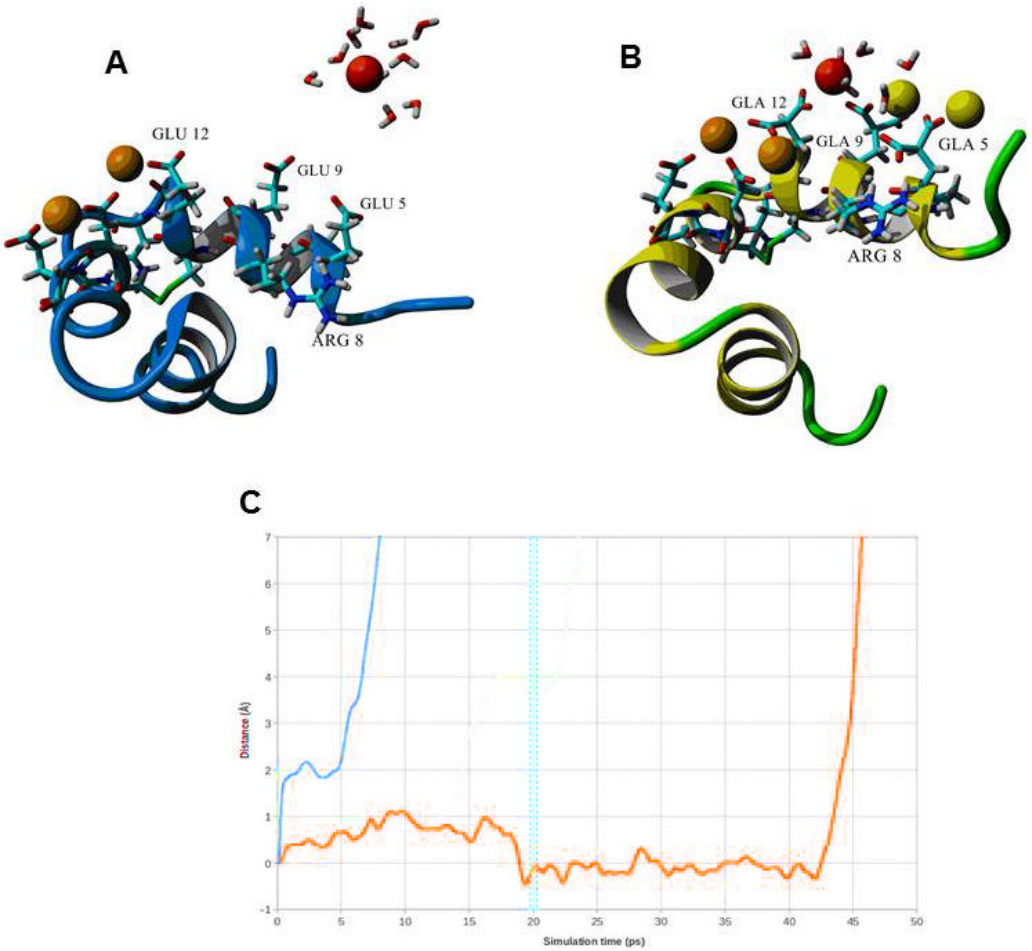

Figure 7. The conformation of Glu-OCN (blue backbone) (A) and Gla-OCN (yellow backbone) (B) after 20 ps of Steered Molecular Dynamics (SM D). The Ca^{2+} ion that was coordinated by Glu or Gla at positions 17 and 21 in Glu-OCON or Gla-OCN is shown as red sphere surrounded by water molecules (red sticks). The remaining two Ca^{2+} ions are shown as orange spheres. Na^{+} counterions are represented as yellow balls. (C) Distance profiles during the SMD runs of Glu-OCN (blue line) and Gla-OCN (yellow line).

saturated with Ca^{2+}, whereas Glu-OCN is expected to be largely in the apo- form (31). Thus, in a physiological scenario, Gla-OCN and Glu-OCN experience a different conformational status and this is of particular importance considering that the endocrine activity of OCN seems to be mediated by the G-protein coupled membrane receptor named GPRC6A (39).

Our results did not investigate the binding of OCN with its putative receptor but address important cues in the investigation dealing with the interaction ligand/modulator-GPRC6A receptor. GPRC6A receptor senses Ca^{2+} via orthosteric binding sites in the long extracellular amino-terminal domain called a Venus flytrap module (VFTM), containing the ligand binding pocket (39). Allosteric modulators, such as osteocalcin, have been hypothesized to bind to distinct sites in the transmembrane domain, influencing or being influenced by Ca^{2+} and other extracellular positive cations, since conformational changes induced by Ca^{2+} binding are suggestive to have important effects on activity threshold of GPRC6A receptor by itself. Pi *et al.*, in fact, showed how, up to 40 ng/ml, osteocalcin had no effect at extracellular Ca^{2+} concentration below 1 mM; thereafter osteocalcin had a dose-dependent effect to stimulate GPRC6A-dependent increments in SRE-luciferase activity in *in vitro* models (40). Thus, precise regulation of extracellular calcium concentration seems to represent a key event in both the modulation of ligand conformation and in receptor sensitivity. Our results on the biochemical behaviour of OCN, related to its differently carboxylated forms, agree with this evidence but further studies are required to confirm the latter observations.

In conclusion, the results of the current study represent a step forward in the comprehension of the role of human osteocalcin as humoral mediator. However, more experimental studies will be necessary to evaluate the actual influence of calcium/OCN binding to the interaction dynamic of ligand with the putative receptor GPRC6A.

6. AKNOWLEDGEMENTS

We thank all the staff of the Human Reproduction Pathology Service for helpful discussions. The authors have nothing to disclose. The atomic coordinates of MD models will be made available upon request.

7. REFERENCES

1. Laizé, V., Martel, P., Viegas, C. S., Price, P. A., and M. L. Cancela: Evolution of matrix and bone gamma-carboxyglutamic acid proteins in vertebrates. *J Biol Chem* 280, 26659-26668 (2005)

2. Hauschka, P. V., Lian, J. B., Cole, D. E., and C. M. Gundberg: Osteocalcin and matrix Gla protein: vitamin K-dependent proteins in bone. *Physiol Rev* 69, 990-1047 (1989)

3. Poser, J. W., Esch, F. S., Ling, N. C., and P. A. Price: Isolation and sequence of the vitamin K-dependent protein from human bone. Undercarboxylation of the first glutamic acid residue. *J Biol Chem* 255, 8685-8691 (1980)

4. Poser, J. W., and P. A. Price: A method for decarboxylation of gamma-carboxyglutamic acid in proteins. Properties of the decarboxylated gamma-carboxyglutamic acid protein from calf bone. *J Biol Chem* 254, 431-436 (1979)

5. Hauschka, P. V., and S. A. Carr: Calcium-dependent alpha-helical structure in osteocalcin. *Biochemistry* 21, 2538-2547 (1982)

6. Delmas, P. D., Stenner, D. D., Romberg, R. W., Riggs, B. L., and K. G. Mann: Immunochemical studies of conformational alterations in bone gamma-carboxyglutamic acid containing protein. *Biochemistry* 23, 4720-4725 (1984)

7. Atkinson, R. A., Evans, J. S., Hauschka, P. V., Levine, B. A., Meats, R., Triffitt, J. T., Virdi, A. S., and R. J. Williams: Conformational studies of osteocalcin in solution. *Eur J Biochem* 232, 515-521 (1995)

8. Dowd, T. L., Rosen, J. F., Li, L., and C. M. Gundberg: The three-dimensional structure of bovine calcium ion-bound osteocalcin using 1H NMR spectroscopy. *Biochemistry* 42:7769-7779 (2003)

9. Hoang, Q. Q., Sicheri, F., Howard, A. J., and D. S. Yang: Bone recognition mechanism of porcine osteocalcin from crystal structure. *Nature* 425, 977-980 (2003)

10. Frazão, C., Simes, D. C., Coelho, R., Alves, D., Williamson, M. K., Price, P. A., Cancela, M. L., and M. A. Carrondo: Structural evidence of a fourth Gla residue in fish osteocalcin: biological implications. *Biochemistry* 44:1234-1242 (2005)

11. Garnero, P.: Biomarkers for osteoporosis management: utility in diagnosis, fracture risk prediction and therapy monitoring. *Mol Diagn Ther* 12, 157-170 (2008)

12. Lee, N. K., Sowa, H., Hinoi, E., Ferron, M., Ahn, J. D., Confavreux, C., Dacquin, R., Mee, P. J., McKee, M. D., Jung, D. Y., Zhang, Z., Kim, J. K., Mauvais-Jarvis, F., Ducy, P., and G. Karsenty: Endocrine regulation of energy metabolism by the skeleton. *Cell* 130, 456-469 (2007)

13. Ferron, M., Hinoi, E., Karsenty, G., and P. Ducy: Osteocalcin differentially regulates beta cell and adipocyte gene expression and affects the development of metabolic diseases in wild-type mice. *Proc Natl Acad Sci U S A* 105, 5266-5270 (2008)

14. Kanazawa, I., Yamaguchi, T., Yamauchi, M., Yamamoto, M., Kurioka, S., Yano. S., and T. Sugimoto: Serum osteocalcin level is associated with glucose metabolism and atherosclerosis parameters in type 2 diabetes mellitus. *J Clin Endocrinol Metab* 94, 3031-3037 (2009)

15. Foresta, C., Strapazzon, G., De Toni, L., Gianesello, L., Calcagno, A., Pilon, C., Plebani, M., and R. Vettor:

Evidence for osteocalcin production by adipose tissue and its role in human metabolism. *J Clin Endocrinol Metab* 95:3502-3506 (2010)

16. Oury, F., Sumara, G., Sumara, O., Ferron, M., Chang, H., Smith, C. E., Hermo, L., Suarez, S., Roth, B. L., Ducy, P., and G. Karsenty: Endocrine regulation of male fertility by the skeleton. *Cell* 144, 796-809 (2011)

17. Pi, M., Chen, L., Huang, M. Z., Zhu, W., Ringhofer, B., Luo, J., Christenson, L., Li, B., Zhang, J., Jackson, P. D., Faber, P., Brunden, K. R., Harrington, J. J., and L. D. Quarles: GPRC6A null mice exhibit osteopenia, feminization and metabolic syndrome. *PLoS One* 3, e3858 (2008)

18. Pi, M., Parrill, A. L., and L. D. Quarles: GPRC6A mediates the non-genomic effects of steroids. *J Biol Chem* 285, 39953-39964 (2010)

19. Karsenty, G., and F. Oury: Biology without walls: the novel endocrinology of bone. *Annu Rev Physiol* 74, 87-105 (2012).

20. De Filippis, V., Vindigni, A., Altichieri, L., and A. Fontana: Core domain of hirudin from the leech Hirudinaria manillensis: chemical synthesis and characterization of a Trp3 analog of fragment 1-47. *Biochemistry* 34:9552-9564 (1995)

21. Molecular Operating Environment (MOE). http://www.chemcomp.com/

22. Ponder, J. W., and D. A. Case: Force Fields for Protein Simulations. *Adv Protein Chem* 66, 27–85 (2003)

23. Case, D. A., Cheatham, T. E., Darden, T., Gohlke, H., Luo, R., Merz, K. M., Onufriev, A., Simmerling, C., Wang, B., and R. J. Woods: The Amber Biomolecular Simulation Programs. *J Comput Chem* 26, 1668–1688 (2005)

24. Hornak, V., Abel, R., Okur, A., Strockbine, B., Roitberg, A., and C. Simmerling: Comparison of Multiple Amber Force Fields and Development of Improved Protein Backbone Parameters. *Proteins* 65, 712–725 (2006)

25. Bradbrook, G. M., Gleichmann, T., Harrop, S. J., Habash, J., Raftery, J., Kalb, J., Yariv, J., Hillier, I. H., and J. R. Helliwell: X-ray and molecular dynamics studies of concanavalin-A glucoside and mannoside complexes - Relating structure to thermodynamics of binding. *J Chem Soc-Faraday Trans* 94, 1603-1611 (1998)

26. Humphrey, W., Dalke, A., and K. Schulten: VMD: visual molecular dynamics. *J Mol Graph* 4, 33-38, 27-28 (1996)

27. RMSD Trajectory tool. http://physiology.med.cornell.edu/faculty/hweinstein/vmdplugins/rmsdtt/

28. Cristiani, A., Brisotto, N., Cedrati, F. C., Floris, M., Scapozza, L., and S. Moro: ClickMD: An Intuitive Web-oriented Molecular Dynamics Platform. *Future Med Chem* 3, 923–931 (2011)

29. Isralewitz, B., Gao, M., and K. Schulten: Steered molecular dynamics and mechanical functions of proteins. *Curr Opin Struct Biol* 11, 224-230 (2001)

30. Brahms, S., and J. Brahms: Determination of protein secondary structure in solution by vacuum ultraviolet circular dichroism. *J Mol Biol* 138, 149-178 (1980)

31. Larsson, L., and S. Ohman: Serum ionized calcium and corrected total calcium in borderline hyperparathyroidism. *Clin. Chem* 24, 1962–1065 (1978)

32. Dill, K. A., Phillips, A. T., and J. B. Rosen: Protein structure and energy landscape dependence on sequence using a continuous energy function. *J Comput Biol* 4, 227–239 (1997)

33. Toma, S., Campagnoli, S., Margarit, I., Gianna, R., Grandi, G., Bolognesi, M., De Filippis, V., and A. Fontana: Grafting of a Calcium-Binding Loop of Thermolysin to Bacillus subtilis Neutral Protease. *Biochemistry* 30, 97-106 (1991)

34. Arnold, F. H., and J. H. Zhang: Metal-mediated protein stabilization. *Trends Biotechnol* 12, 189–192 (1994)

35. De Filippis, V., De Dea, E., Lucatello, F., and R. Frasson: Effect of Na^+ Binding on the Conformation, Stability, and Molecular Recognition Properties of Thrombin. *Biochem J* 390, 485-492 (2005)

36. Matthews, B. W., Nicholson, H., and W. J. Becktel: Enhanced protein thermostability from site-directed mutations that decrease the entropy of unfolding. *Proc Natl Acad Sci USA* 84, 6663-6667 (1987)

37. Polverino de Laureto, P., Scaramella, E., De Filippis, V., Marin, O., Doni, M. G., and A. Fontana: Chemical Synthesis and Structural Characterization of the RGD-Protein Decorsin: a Potent Inhibitor of Platelet Aggregation. *Protein Sci* 7, 433-444 (1998)

38. Nishimoto, S. K., Waite, J. H., Nishimoto, M., and R. W. Kriwacki: Structure, activity, and distribution of fish osteocalcin. *J Biol Chem* 278, 11843-11848 (2003)

39. Pi, M., and L. D. Quarles: Multiligand specificity and wide tissue expression of GPRC6A reveals new endocrine networks. *Endocrinology* 153, 2062-2069 (2012)

40. Pi, M., Faber, P., Ekema, G., Jackson, P. D., Ting, A., Wang, N., Fontilla-Poole, M., Mays, R. W., Brunden, K. R., Harrington, J. J., and L. D. Quarles: Identification of a novel extracellular cation-sensing G-protein-coupled receptor. *J Biol Chem* 280, 40201-40209 (2005)

Key Words: Osteocalcin, Calcium Metabolism, Gamma-Carboxylation, Circular Dichroism, Protein Stability, Calcium-Binding Proteins, Molecular Dynamics

Send correspondence to: Carlo Foresta, Department of Molecular Medicine, Section of Clinical Pathology and Centre for Human Reproduction Pathology, University of Padova, Via Gabelli 63, 35121 Padova, Italy, Tel 39-49-8218517, Fax: 39-49-8218520, E-mail: carlo.foresta@unipd.it